Advanced Steel Construction – Vol. 20 No. 1 (2024) 93–104
DOI:10.18057/IJASC.2024.20.1.10

AN INVESTIGATION ON THE EFFECT OF RANDOM PITTING CORROSION ON THE STRENGTH OF THE SUBSEA PIPELINE USING MONTE CARLO METHOD

Tong Lin [1] , Wei Huang [1,*] , Si-Wei Liu [2] and Rui Bai [1]

[1] *School of Civil Engineering, Sun Yat-Sen University, Guangzhou, China*
[2] *Department of Civil and Environmental Engineering, The Hong Kong Polytechnic University, Hung Hom, Kowloon, Hong Kong, China*
* (*Corresponding author: E-mail: huangw288@mail.sysu.edu.cn*)

ABSTRACT

Pitting corrosion is normally distributed randomly along the pipeline, which is the source of the uncertainty affecting the ultimate bearing capacity of the submarine pipelines. So the Monte Carlo method is employed to study the effect of pitting corrosion on the upheaval buckling behavior of the pipeline. A corroded pipeline model with randomly distributed pitting corrosion is utilized to captures the intricate realities of corrosion scenarios. Multiple corrosion models with distinct artificial patterns have been meticulously crafted. Additionally, a new pipeline element based on Euler-Bernoulli beam theory is extended considering corroded sections, pipe-soil interactions, axial load, initial imperfections, and other major factors. Moreover, the bearing capacity, vertical deformation and section stress of the pipeline under corrosion is discussed thoroughly, wherein a Newton- Raphson typed numerical analysis procedure is utilized for nonlinear analysis of the upheaval buckling of pipelines. The influence of corrosion parameters such as the corrosion depth, corrosion ratio and area loss ratio on mechanical properties of the submarine pipelines is further analyzed in detail. It's indicated that varying patterns of corrosion distribution, despite exhibiting identical corrosion parameters, can result in distinct reduction factors and vertical buckling displacements.

ARTICLE HISTORY

Received: 20 February 2024
Revised: 20 March 2024
Accepted: 20 March 2024

KEYWORDS

Monte Carlo method;
Corrosion;
Pipeline element;
Upheaval buckling;
Submarine pipelines

1. Introduction

Submarine pipelines are highly efficient in transporting oil and gas, also recognized as "lifeline engineering", as they play a similar role as human arteries. However, the complexity of the marine environment results in corrosion in steel pipelines, leading to pipeline failures and damage. The corrosion of pipelines not only compromises their structural integrity but also poses potentially harmful consequences for the surrounding marine environment. Pitting corrosion is a common form of localized corrosion that occurs due to inadequate cathodic protection or absence of pipeline coating. The phenomenon is characterized by the formation of small pits on the pipeline surface, which can grow in size and depth, leading to severe pipeline damage over time. Pitting damage, though diminutive in size, can trigger the stress concentration and expedite the onset of plasticity in metallic structural components. To mitigate such corrosion-related concerns, it's imperative to ensure a robust coating system and effective cathodic protection measures are in place. It's therefore imperative to remain vigilant and implement effective maintenance strategies to detect and preserve against such damages to ensure the durability and longevity of structures[1-3].

Submarine pipelines installed on uneven seabeds are prone to buckling when exposed to elevated temperature and pressure conditions. Thermal expansion and pressure increase can generate axial compression force that exceeds the pipeline's critical axial compression limit. This exceeds the stress and strain thresholds, potentially resulting in local buckling and decreased axial carrying capacity, which may even lead to fatigue and fracture[4,5]. It's essential to proactively mitigate such risks by applying adequate pipeline design methods and advanced modelling techniques to anticipate and prevent corrosion failure to safeguard the pipeline's functioning and longevity. When pipelines undergo corrosion, there is an increased risk of compromised structural integrity and strength, resulting in uncertainty regarding the estimation of burst pressure. Consequently, it is crucial to evaluate the impact of corrosion on the pipeline's buckling behavior. Nevertheless, the corrosion of pipelines is influenced by several factors such as the ocean environment, anti-corrosion effect, pipeline materials and manufacturing technology, stress level etc. Meanwhile, the specific feature and geometric parameter of pitting corrosion including the corrosion ratio, distribution, size and shape are of great variability, which leads to the uncertainties of its adverse effects on the performance of steel pipelines. There is a possibility of encountering challenges during the design and operation of submarine pipelines.

Pitting corrosion in pipelines is typically marked by the formation of circular cavities on the exterior of the compromised material. These cavities are typically assumed to be of uniform or random size, depth, and distribution throughout the pitted member [6]. The Pipeline Defect Assessment Manual (PDAM) offers a comprehensive overview of the techniques available for evaluating pipeline flaws, including corrosion. Additionally, it highlights a specific defect type and the associated factors that contribute to uncertainty in the modeling process for each assessment [7]. Netto [8] developed a numerical tool by creating oval corrosion pits defects for pipelines through the process of spark corrosion while the size and area of defects was specified, and the influence of corrosion defects on the collapse pressure of offshore pipelines was studied. Wang et al.[9] introduced random pitting defects into the outer surface of the pipeline by using 6% ferric chloride solution and found that the shape of pitting defects was cylindrical or semi-ellipsoid. It is said that the random geometric defects, amplitude of out-of-roundness and material properties would affect the collapse pressure significantly. Motta et al.[10] evaluated the failure pressure of corroded pipelines using nonlinear FE analyses of the manufactured defect models with constant or complex shape, dimension and configuration which were generated by PIPEFLAW. It is said that the conservative predictions would be obtained based on the semiempirical method. Mohd et al.[11] conducted a study on the residual strength properties of corroded subsea pipelines subjected to combined internal pressure and bending moment, taking into account the distinct characteristics (distribution, shape, and size) of the corrosion models. Nazaria et al.[12] used an idealized corrosion model in elliptical shape with 16 different corrosion geometries varied in depth, length and location along the tube aiming for predicting the ultimate strength and buckling behavior of locally damaged tubes. Ahn et al.[13] conducted compressive loading tests on steel tubes with two different types of artificially induced corrosion damage achieved by a mechanical process to examine the residual compressive strength and structure of locally corroded tubes. In reality, corrosion damage in pipelines is frequently more intricate than idealized models assume, as they postulate a uniform distribution of corrosion pits. While these simplified models may offer some insights into the underlying mechanisms of corrosion, they tend to overestimate the pipeline's strength under the same level of corrosion scenarios in reality. Therefore, the utilization of models that accurately replicate the dispersion of pitting corrosion is imperative, along with a thorough examination of the potential mechanisms of pipeline failure across varying corrosion scenarios [3]. Those equations derived from specific corroded models or actual corroded members should be examined for applicability in practical use. This is owing to the lack of consideration of the uncertainties associated with the various features of pitting corrosion, as evenly corroded surfaces with uniform corrosion dimensions are rare in reality [14, 15]. The presence of uncertainties in the corrosion features of pipelines can lead to variations in their ultimate strength. To accurately determine the remaining strength of corroded components, it is necessary to employ simulation technologies that can replicate the real-world conditions of the pipelines. Without such simulations, it is difficult to draw general conclusions about the strength of corroded components under different loading scenarios, as the impact of corrosion can vary greatly depending on the specific materials,

conditions, and geometries involved [16].

The present study aims to examine the impact of various corrosion parameters, including distribution, shape, and size, on the ultimate strength of submarine pipelines exposed to severe corrosive environments [6, 17-21]. Chen et al.[17] presented an efficient algorithm to determine the deterioration of the bearing cpacitys of I-Section steel members with random corrosion. Silva et al.[18] conducted a study on the diverse forms of corrosion, examining the influence of a random distribution of corrosion thickness on the ultimate strength of an unstiffened rectangular steel plate. Wang et al.[19] analyzed the failure mechanism and degradation of ultimate strength of the plated steel structure caused by the random pitting corrosion. A numerical study was carried out on tubular members of diverse slenderness ratios with pitting corrosion on the surface along the length and hoop to clarify the pitting effect on ultimate strength [6]. Ben et al.[20] applied Separable Monte Carlo (SMC) for randomly sampling the sets of input parameters of the Limit State Function (LSF) for the purpose of estimating the failure probability of corroded pipelines.

Pipelines play a critical role in transportation of oil and gas products in the subsea environment [22-25]. Owing to the unpredictable nature of pitting distribution and the intricate variations in material properties, considerable uncertainty persists regarding the impact of corrosion on the bearing capacity of pipelines. Hence, the aim of this research is to utilize the Monte Carlo method to investigate the upheaval buckling of submarine pipelines that are influenced by pitting corrosion, considering its stochastic distribution. A new pipeline element based on the Euler-Bernoulli beam theory to investigate the impact of pitting corrosion on submarine pipelines, including its random distribution across the cross-section, length, and circumference of the pipeline. A detailed explanation of how to employ these effects into the pipeline element is presented in detail. It is essential to consider the impact of pitting corrosion on the pipeline's overall bearing capacity as it significantly affects its performance. This paper is structured as follows, Section 2 explains the submarine pipeline model considering the pitting corrosion in detail. Utilizing the Monte Carlo method, a significant number of corrosion sections are randomly produced and organized to accurately replicate the dispersal pattern of pitting corrosion across both the longitudinal length and the circumferential perimeter of the pipeline surface. Section 3 provides a detailed description of the computational methods employed for determining the pertinent parameters of corroded submarine pipelines. The sections were discretized, and the geometric parameters were computed in accordance with the pertinent section model. Section 4 presents the flowchart of buckling analysis of the corroded pipeline. Sections 5 to 7 offer a detailed exposition on the determination of the bearing capacity, vertical deformation, and stress of corroded pipelines. The buckling behavior of pipelines affected by corrosion is discussed extensively. Moreover, parameter analysis that examines how the size and type of corrosion affects the buckling deformation as various pipeline types is presented. The concluding remarks are subsequently summarized.

2. Corrosion modelling of the pipeline

In our previous works, a new pipeline element based on the Euler-Bernoulli beam theory designed for pipeline buckling analysis has been proposed [26-28]. Compared to the traditional method that utilizes Winkler-type springs to account for soil-pipeline interaction, it has been demonstrated that the method we proposed is more efficient. This advantage becomes more apparent when using the Monte Carlo method, as it requires the design and execution of numerous cases. By considering the corrosion distribution across the cross-section, length, and circumference of the pipeline, section properties can be determined. This part provides a detailed explanation of how pitting corrosion is distributed on the pipeline.

In most conditions, features of pitting corrosion are randomly distributed in steel pipelines due to the harsh ocean environment. Regardless of the shape of the pits, corrosion at the sectional level results in a decrease in the thickness of the section. Fig.1 shows the generation of the corrosion model of a pipeline cross section. The circular hollow section of the pipeline can be described using two variables i.e. wall thickness *t* and diameter *D*.

Divide the pipeline cross section into *n* small segments with the same radian θ. Those corroded segments will be chosen by random, and the thickness of the corroded segments t_r will be expressed as,

$$t_r = t - t_d \tag{1}$$

where *t* is the wall thick of the pipeline, t_d is the corrosion depth of the chosen segment, which is randomly distributed in reality.

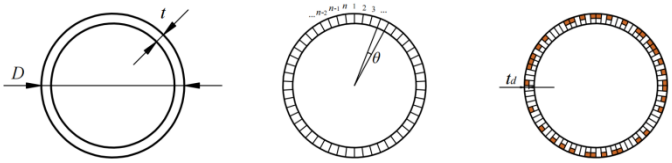

Fig. 1 The generation of the corrosion on a pipeline cross section

The total number of corroded segments n_c can be expressed as,

$$n_c = n\rho_{CR} \tag{2}$$

where n_c denotes the number of segment and ρ_{CR} is the corrosion ratio which represents the proportion of corroded segments to the total number of intact segments within a given section.

Thus, the area loss ratio of the section (DOPs) can be deduced,

$$\text{DOPs} = \frac{A_c}{A} = \frac{0.5\theta t_d(D - t_d)}{(D - t)\pi t} n\rho_{CR} \tag{3}$$

where *A* and A_c are the original area and corroded area of the cross section. DOPs indicates the pitting intensity of the cross section.

In Monte Carlo simulation, all corrosion sections are arranged along the length of the pipeline, so pitting corrosion is distributed on the surface of the pipe along the length and circumferential direction of the pipeline. In other words, the pipeline is divided into *m* small segments with the same length *l* along the pipeline axis, where *m* also means the number of runs for the Monte Carlo simulation, as shown in Fig. 2. It is important to note that the cross-section of the pipeline can be subdivided into numerous extremely small cross-sectional segments, each with a negligible volume. These corrosion segments are randomly distributed and combined, resulting in the formation of pitting corrosion, the volume and shape of which are inherently unpredictable so as to captures the intricate realities of corrosion scenarios.

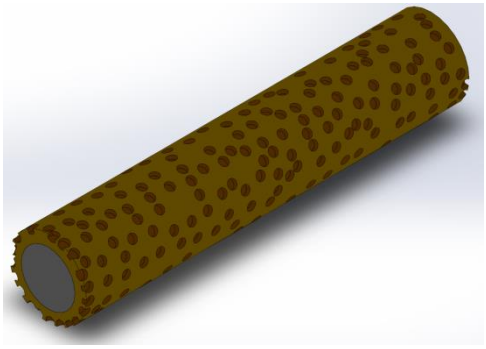

(a) A pipe with random pitting corrosion

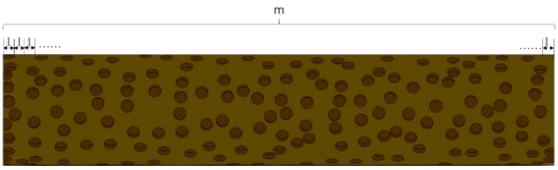

(b) The dimension of pitting corrosion

Fig. 2 Pipeline model with corrosion

The degree of degradation (DOD) is introduced to describe the deterioration of the pipeline, which can be expressed as,

$$\text{DOD} = \frac{V - V_r}{V} \tag{4}$$

where V and Vr are the original volume and remaining volume of the pipeline, which can be obtained by[29],

$$V = (D - t)\pi t L \tag{5}$$

$$V_r = [(D-t)\pi t - 0.5\theta t_d(D-t_d)n\rho_{CR}]L \quad (6)$$

$$\mathrm{DOD} = \frac{0.5\theta t_d(D-t_d)n\rho_{CR}L}{(D-t)\pi tL} \quad (7)$$

3. Bearing capacity and relevant parameters

3.1. Bearing capacity

The bearing cpacity of steel pipelines are discussed in this section. To assess the pipeline's structural integrity, axial compression force *P* is applied uniformly to both ends. It should be noted that both ends of the pipelines are fixed when estimating the bearing capacity of the pipelines under axial compression. Subsequently, the external load is incrementally increased until the stress concentration at a designated cross-sectional point achieves the yield strength. This approach allows for an accurate assessment of the pipeline's resistance to failure under compressive loads. When the yield strength is reached, the pressurization is stopped and the maximum pressure applied is collected as the bearing capacity. Global buckling of pipelines can be approximately considered as a column-type response, given the restricted deformation of their cross-sections. As a result, the Euler buckling approach is a suitable method to analyze their buckling behavior [23, 30]. The criteria for pipeline failure pressure in the commonly used evaluation criteria at home and abroad can be summarized into two categories: two failure criteria based on stress and strain [2]. The evaluation criteria commonly utilized domestically and internationally for pipeline failure pressure can be categorized into two principal branches: stress-based and strain-based failure criteria[31]. In engineering practice, however, the deformation of pipeline sections is frequently constrained by various factors, including material strength, manufacturing processes, and operational environments. Consequently, the degree of deformation is typically limited, making the stress-based failure criterion the prevailing approach for assessing the bearing capacity of pipelines with corrosion defects. Therefore, this study opts to employ the stress-based failure criterion for calculating the load-bearing capacity of pipelines with corrosion defects.

The yield strength is a commonly used evaluation index for the mechanical properties of solid materials, representing the practical limit of the material's use. When stress surpasses the yield limit, plastic deformation occurs, leading to a sudden increase in strain and eventual failure of the materia. According to ASME B31.4-2022 [32], the longitudinal stress from pressure and external loadings in unrestrained pipe is calculated by,

$$S_L = \frac{P_i D}{40t} + \frac{iM}{Z} + \frac{F_a}{A} = \frac{P_i D}{40t} + \frac{F_a}{A} + \frac{My_{max}}{I} \le 0.54S_y \quad (8)$$

where, A is the section area, M is the bending moment across the nominal pipe cross section due to weight or seismic inertia loading, y_{max} is the maximum distance to axis on the section, S_y is the specified minimum yield strength of pipeline material, F_a is the axial force, P_i is the internal design gage pressure, Z is the section modulus of the pipeline, i is the component stress intensification in plane of loading, limited by $0.75i \ge 1$. For straight pipe, i=1.0.

The bearing cpacity P_B of the steel pipeline under compression can be expressed as,

$$P_B = AS_L \quad (9)$$

3.2. Relevant geometrical parameters

In order to calculate the bearing capacity in Eq. (8), the pertinent section parameters of the pipeline should be confirmed firstly. Due to the randomness of corroded sections, their area, centroid coordinates, and moment of inertia must be calculated using a fiber model. In this model, each unit of the section is treated as a fiber, with its centroid coordinates and area calculated and stored as small fiber blocks. By integrating all of these fiber blocks, the full fiber model information for the entire corroded section can be obtained, which includes the section area *A*, the centroid coordinate (Y_0, Z_0) and the moment of inertia *I*. A coordinate system *yoz* is established to describe the position of each node, where the centroid of the cross-section is *o*, as shown in Fig. 3. According to the equations above, the section area *A*, centroid coordinates (Y_0, Z_0) and the moment of inertia *I* are key parameters for the computation of bearing cpacity of corroded section. They are given by,

$$t_{ri} = \begin{cases} t & \text{(uncorroded)} \\ t - t_d & \text{(corroded)} \end{cases} \quad (10)$$

$$R_i = \frac{D}{2} - t + \frac{t_{ri}(1.5D - 3t + 2t_{ri})}{3(D - 2t + t_{ri})} \quad (11)$$

$$A_i = 0.5\theta t_{ri}(D - 2t + t_{ri}) \quad (12)$$

$$A = \sum_{i=1}^{n} A_i \quad (13)$$

$$Y_0 = \sum_{i=1}^{n} Y_i A_i / A = \sum_{i=1}^{n} R_i \sin\phi_i A_i / A \quad (14)$$

$$Z_0 = \sum_{i=1}^{n} Z_i A_i / A = \sum_{i=1}^{n} R_i \cos\phi_i A_i / A \quad (15)$$

$$I_y = \int (Z_i - Z_0)^2 dA = \frac{\theta}{2}\sum_{i=1}^{n} (R_i \sin\phi_i - Z_0)^2 t_{ri}(D - 2t + t_{ri}) \quad (16)$$

$$I_z = \int (Y_i - Y_0)^2 dA = \frac{\theta}{2}\sum_{i=1}^{n} (R_i \cos\phi_i - Y_0)^2 t_{ri}(D - 2t + t_{ri}) \quad (17)$$

where: I_y and I_z are the *y*- and *z*- moment of inertial of the asymmetric section after corrosion. R_i denotes the length from the left node of i_{th} segment on the cross section to the center *o*, while ϕ_i denotes the angle between the line and *y* axis, as shown in Fig. 4.

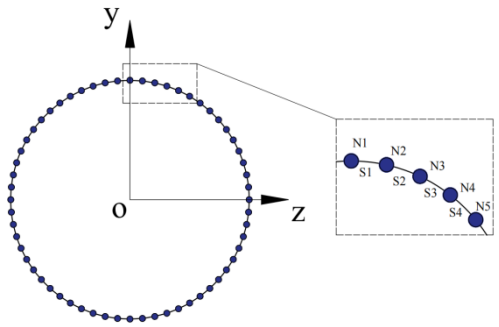

Fig. 3 Corroded section division and the number

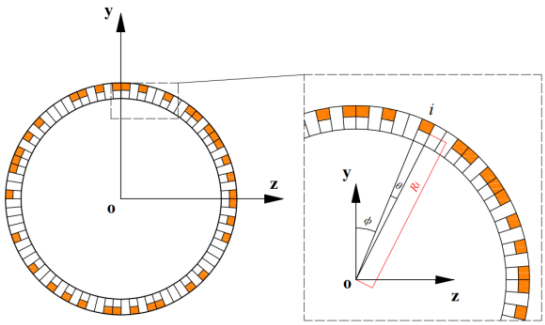

Fig. 4 Segments on the corroded section

4. Flowchart of buckling analysis

The detailed flowchart of how to perform the buckling analysis is presented in Fig. 5. The section is divided into *n* segments, and the central angle of each unit is θ. The number of corroded pieces n_c can be calculated based on Eq. (2). Several ϕ_i $(i = 1, 2, 3 \ldots n)$ locating the positions of corroded pieces are

generated randomly, which guarantees the random properties of pitting corrosions. When the pits and section parameters are obtained for *m* cases, the buckling analysis based on the Newton-Raphson iteration procedure is carried out. The internal pressure and external hydrostatic pressure of the pipeline are expressed by the pressure difference. The vector sum of the pipeline internal pressure, external hydrostatic pressure and the external load applying at both ends of the pipeline element is named as external forces, which can be seen in Fig.5. The python program stops running and records the utmost permissible loading pressure as the pipeline's bearing capacity when the normal stress on a section of the pipeline exceeds its yield strength, indicating that the pipeline is damaged and can no longer withstand the compressed pressure.

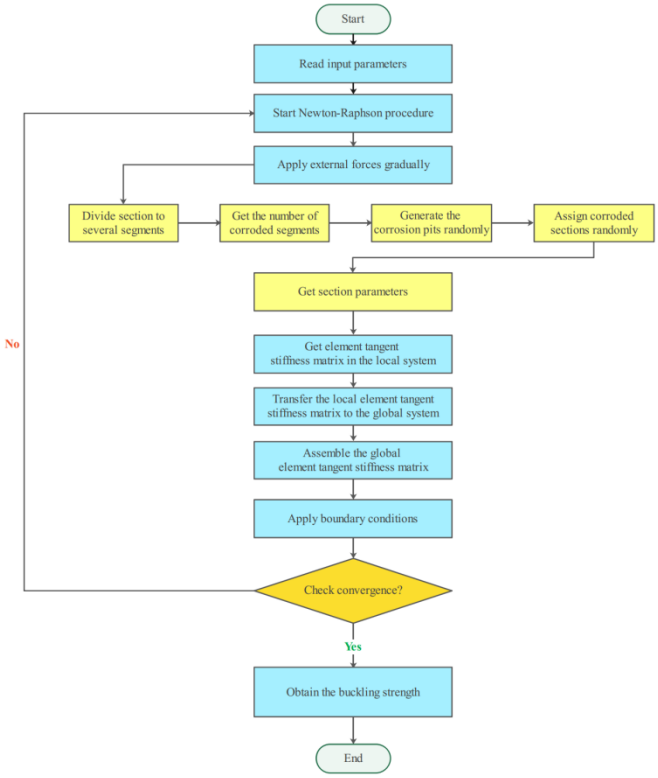

Fig. 5 Flow chart of the Monte Carlo simulation procedure

5. Monte Carlo simulation

5.1. Design parameters of the pipeline

The basic information of section's size, corrosion ratio, corrosion depth and segments are shown in Table 1.

Table 1
Design parameters for the pipeline and corrosion

Description	Paramete	Value	Unit
Diameter	D	323.9	mm
Thickness	t	14.3	mm
Pipeline length	L	100	m
Number of segments	n	360	-
Mesh size	θ	1	◦
Corrosion ratio	ρ_{CR}	50	%
Corrosion depth	t_d	2.86	mm
Initial imperfection length	L_{Y0}	20	m
Initial imperfection amplitude	V_{m0}	0.2	m
Young's module	E	206	GPa
Yield strength	S_y	450	MPa
Length coefficient	k	1	-
Total number of pipeline element	n_{ele}	300	-

The pipelines are fabricated by an API 5L X65 PSL2 steel and both ends of the pipelines are assumed fixed, the initial imperfection of the pipeline can be determined by the following equation,

$$V_0(X) = \frac{V_{m0}}{2}[1 + cos(\frac{2\pi}{L_{Y0}})], \quad -\frac{L_{Y0}}{2} < X < \frac{L_{Y0}}{2} \tag{18}$$

where, V_{m0} is the maximum initial imperfection amplitude about *Y*- axis, as shown in Fig. 6; L_{Y0} is the vertical initial imperfection length. The pipeline is assumed to be placed in a trench on a semi-rigid seabed and covered with backfill soil. The sum weight of the trench backfills and the pipeline is 1.5 kN/m and the vertical soil-pipeline interaction can be obtained and presented in Fig. 7. The axial friction between the pipeline and the foundation is ignored. The specific parameters of the damaged pipeline model are shown in the Table 1. 2000, 4000, 6000, 8000 and 10000 kN load are divided into 100, 1000, 2500 and 5000 parts and applied on both ends of the pipeline element. The step length and bearing capacity of each test are recorded in Table 2. Arrange the bearing capacity in Table 2 into Table 3 according to the load step and record the the run time of the program of different load steps. For different applied loads, when the same step size is set, the calculation results are basically similar. When the step length is in the range of 4 ~ 6 kN, the absolute value of the relative error between the bearing capacity and the high-precision result is less than 0.5%, which is acceptable. Indeed, the computation time for all scenarios remains minimal, with the longest duration being less than 16 minutes. Therefore, the step length can be taken as 4 ~ 6 kN in the case studies in the following sections.

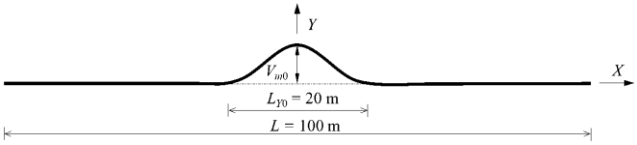

Fig. 6 Initial vertical configuration of the pipeline

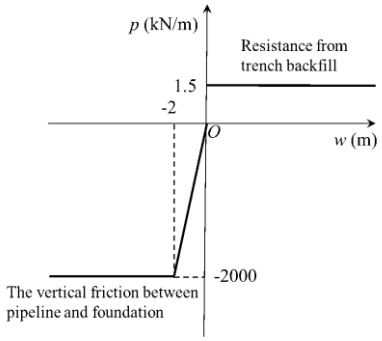

Fig. 7 Pipe-soil interaction

5.2. Run time assessment of Monte Carlo simulation

Monte Carlo method is conducted to simulate a naturally corroded pipeline, and numerous cases are needed to be carried out. To establish the relationship between the Monte Carlo simulation outcomes (bearing capacity) and the number of runs, investigations on bearing capacity, number of runs, and pipeline slenderness are necessary. The basic information of section's size, corrosion ratio, corrosion depth and segments are kept the same with Section 5.1. The Monte Carlo simulation is then performed several times for each type of pipeline according to different slenderness of the pipeline. Slenderness is the ratio of the pipeline length to the radius of rotation of the pipeline Section. For the uncorroded pipelines, it is given by,

$$\lambda = \mu\frac{L}{R_{gr}} = \mu\frac{L}{\sqrt{I/A}} = \mu\frac{4L}{\sqrt{D^2 + d^2}} \tag{19}$$

where, μ is the length factor, for pipeline with both ends fixed, μ=0.5; R_{gr} is the radius of gyration of the Section; *d* is the inner diameter of the pipeline. The slenderness is determined according to the size of the pipeline before being corroded and the estimated bearing capacity is documented accordingly.

Table 4 presents the bearing capacity of 9 pipelines with length of 30m,

50m, 100m, 150m, 200m, 250m, 300m, 400m and 500m at different random times and record the results with random times of 50, 100, 300, 500 and 1000 respectively. Fig. 8 shows that the bearing capacity of the pipeline decreases as the slenderness increases. For pipelines with slenderness of 245.7, 409.5, 819.0, 1228.5 and below, the bearing capacity decreases rapidly as the pipeline length increases. For pipelines with the slenderness of 1638.0, 2047.5, 2457.0, 3276.0, 4095.0 and above, the bearing capacity is limited by length of the pipeline. In this scenario, as the slenderness (pipeline length) increases further, the reduction in bearing capacity of the pipeline gradually stabilizes, ultimately resulting in a consistent and reliable bearing capacity value.This significant effect on the buckling behavior due to the pipeline length was also found by other researchers [24]. One of their results shows that, for long pipelines, if the pipeline length is greater than the critical length, the increase of pipeline length has negligible effect on the analysis results. As the area loss rate of the section remains constant in each turn, the resulting maximum and minimum bearing capacities should also be consistent across different runs. The calculated results of cases with a run count of 1000 were used as reference values. Upon achieving a run count of 300, the relative error between the pipeline's bearing capacity and the reference value remains consistently below 2%. To ensure efficient computation and avoid unnecessary delays, we have elected to limit the number of random iterations to a range of 300 to 500 runs in the scenarios outlined below.

Table 2
Loading condition of the pipeline with corrosion

Load step	100		1000		2500		5000	
Member load (kN)	Step length (m)	Bearing capacity (kN)	Step length (m)	Bearing capacity (kN)	Step length (m)	Bearing capacity (kN)	Step length (m)	Bearing capacity (kN)
2000	20	1140	2	1138	0.8	1137.6	0.4	1138.4
4000	40	1160	4	1140	1.6	1137.6	0.8	1137.6
6000	60	1140	6	1140	2.4	1140.0	1.2	1135.2
8000	80	1120	8	1144	3.2	1139.2	1.6	1139.2
10000	100	1200	10	1140	4.0	1136.0	2.0	1140.0

Table 3
Run time and relative error of different load steps

Load step (kN)	Run time (min)	Relative error (%)	Load step (kN)	Run time (min)	Relative error (%)
100	<0.5	5.411	4.0	16	0.141
80	<1	1.620	3.2	22	0.070
60	<1	0.141	2.4	31	0.141
40	<1	1.897	2.0	55	0.035
20	<2	0.141	1.6	98	0.070
10	<5	0.141	1.2	122	0.281
8	<7	0.492	0.8	190	0.070
6	<8	0.141	0.4	360	0.000

Table 4
The pipeline bearing capacity related to run time of Monte Carlo simulation

Run count		50		100		300		500		1000	
Length (m)	Slenderness	Bearing capacity (kN)	Relative error (%)	Bearing capacity (kN)	Relative error (%)	Bearing capacity (kN)	Relative error (%)	Bearing capacity (kN)	Relative error (%)	Bearing capacity (kN)	Relative error (%)
30	245.7	1494	4.96	1560	0.76	1572	0.00	1560	0.76	1572	0.00
50	409.5	1326	0.00	1332	0.45	1326	0.00	1326	0.00	50	409.5
100	819.0	1140	0.00	1140	0.00	1140	0.00	1140	0.00	100	819.0
150	1228.5	1056	1.68	1080	0.56	1080	0.56	1080	0.56	150	1228.5
200	1638.0	1026	1.72	1050	0.57	1044	0.00	1044	0.00	200	1638.0
250	2047.5	1050	2.34	1032	0.58	1026	0.00	1026	0.00	250	2047.5
300	2457.0	1008	0.60	1020	1.80	1014	1.20	1002	0.00	300	2457.0
400	3276.0	1020	1.80	1008	0.60	1002	0.00	1002	0.00	400	3276.0
500	4095.0	1002	1.21	1020	3.03	990	0.00	990	0.00	990	0.00

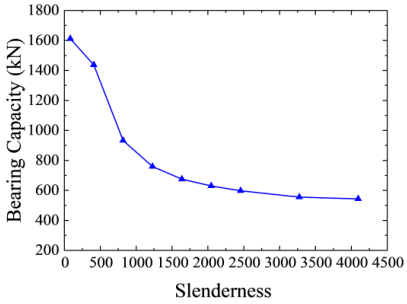

Fig. 8 The bearing capacity of pipelines with different slenderness

5.3. Bearing capacity of specified corrosion models

Monte Carlo Simulation constructs models of potential outcomes by utilizing probability distributions, like the uniform or normal distribution, to account for variables that have inherent uncertainty. This enables the prediction of a range of results based on estimated values. Although two pipeline models may have the same size, corrosion ratio, corrosion depth, and other corrosion-related parameters, they are essentially distinct models because of the different corrosion pitting layout. In order to figure out the difference of the bearing capacity of pipelines caused by the randomness of corrosion distribution, six different corrosion patterns are artificially designed, as shown in Fig. 9. In Type *a*, the regularly distributed corrosion pattern is assumed, in which the section is symmetrical about both vertical and transverse axes. In Types *b* and *c*, the

corrosion only distributes at the left half and right half, respectively. In Type *d* and *e*, the corrosion only distributes at the top half and bottom half, respectively. In Type *f*, an irregularly distributed corrosion pattern is adopted. The basic information of section's size, corrosion ratio, corrosion depth and segments are shown in Table 5. The area loss ratios of the sections with different corrosion patterns are all 81.37%. Table 6 presents the bearing capacity of six types of pipelines. The distribution of corrosion in a pipeline plays a crucial role in determining its buckling bearing capacity, which can vary considerably.

In particular, Types *d* and *e* tend to have the smallest buckling bearing capacity. By analyzing corrosion distribution, we can identify the most dangerous types and take necessary measures to avoid them in practical engineering, reducing the risk of damage.

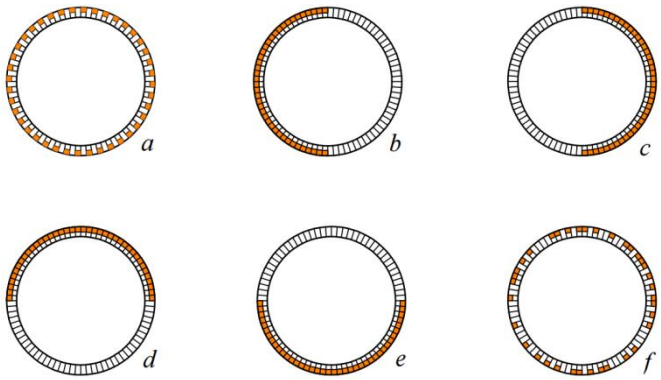

Fig. 9 Specified corrosion models

Table 5
Design parameters for the pipeline and corrosion

Description	Paramete	Value	Unit
Diameter	D	200	mm
Thickness	t	30	mm
Pipeline length	L	100	m
Number of segments	n	360	-
Mesh size	θ	1	◦
Corrosion ratio	ρ_{CR}	50	%
Corrosion depth	t_d	10	mm
Initial imperfection length	L_{Y0}	20	m
Initial imperfection amplitude	V_{m0}	0.2	m
Young's module	E	206	GPa
Yield strength	S_y	450	MPa
Length coefficient	k	1	-
Total number of pipeline element	n_{ele}	300	-

Table 6
Bearing capacity of different corrosion type

Corrosion type	*a*	*b*	*c*	*d*	*e*	*f*
Bearing capacity (kN)	1044	1032	1032	1020	1026	1044

5.4. The influence of the maximum wheelbase of the section

According to the equations in Section 3.1, the maximum wheelbase on the section y_{max} is an important parameter when calculating the section coefficient W_Z, and its size directly affects the normal stress of the section. However, since numerous corroded sections are distributed along the length of the pipeline, the section parameters of each pipeline element are different and uncertain. Meanwhile, the value of y_{max} for corroded pipelines is not defined in the relevant specifications. In other words, the section coefficient W_Z of each piping element is also indeterminate, reflecting the real-world conditions. To assess the impact of uncertainty in W_Z on the calculated magnitude of normal stress in a given section, a comprehensive case study was undertaken.

Five pipeline section models with different sizes are designed and the corroded levels of these sections are unified. The specific parameters of these corroded pipeline models are the same with Section 5.3. In the pipeline element program, the y_{max} value is taken as $D/2$ and $D/2$-t_d respectively, which represents the maximum wheelbase of the section before and after corrosion. The bearing capacity of these corroded pipelines of each case is recorded in Table 7. Take the minimum bearing capacity of all the cases as the reference, the relative error of each case compared with the reference value can be obtained. At the same time, the bearing capacity of these five pipelines with intact section (no corrosion) is also presented.

It can be seen from Table 7 that as the thickness-diameter ratio of the pipeline decreases, the relative error of the bearing capacity of the pipeline caused by the value of y_{max} gradually decreases. The difference between the calculation results of the corroded pipeline model and the non-corroded pipeline model is gradually becoming smaller. For the corroded pipeline with thicker wall, when y_{max} equals $D/2$, the bearing capacity of the pipeline is the smallest among all the cases. Compared with the bearing capacity of the non-corroded pipeline in the same size, the bearing capacity of pipeline buckling obtained for two different values of wheelbase of cross-section is obviously different.

In the following studies, the value of y_{max} are considered as $D/2$ and $D/2$-t_d separately, and the pipeline bearing capacity under two maximum wheelbase values are referred as low value and high value. For the thin-walled pipelines, the relative errors between the bearing capacity of the corroded pipeline and the uncorroded one are smaller than that of thick wall pipelines. When the pipeline wall is thin and the thickness-diameter ratio is relatively small, the bearing capacity is determined mainly by its size. Slight corrosion has little effect on the bearing capacity of the pipeline, so the difference of pipeline bearing capacity before and after the corrosion shrinks.

6. Buckling bearing capacity assessment

This section aims at examining the distinct impact of varying parameters of corrosion on pipeline bearing capacity, while also comparing the effects of corrosion on pipelines of different sizes. Three pipeline sections with different sizes were selected according to ASME specifications, and their related parameters are presented in the Table 8. The pipeline element is limited to static analysis at present and does not involve dynamic analysis. Therefore, hydrodynamics cannot be considered temporarily. The pipelines are all single-walled in this paper. This method is not applicable for the buckling analysis of PIPs or piggyback pipelines at present. The thickness-diameter ratio of three kinds of pipelines is, Type 3> Type 1> Type 2. As vital parameters related to corrosion, the corrosion depth and corrosion ratio are set as variables. The corresponding DOPs are also presented to reflect the overall effect of corrosion on the bearing capacity of pipeline. The corrosion depth of the pipeline section varies between 20%, 40%, 60%, and 80% of its original thickness. Concurrently, the corrosion ratio fluctuates between 0.2, 0.4, 0.6, and 0.8 of the total number of elements comprising the pipeline section. It should be noted that the corrosion depth ratio is the ratio of corrosion depth to the original thickness of the section. Both high and low values of the bearing capacity are presented respectively in Tables 9 and 10. The specific parameters of these corroded pipeline models are consistent with Section 5.3.

Table 8
Design parameters for the pipeline section model

Parameters	Type 1	Type 2	Type 3
D (mm)	323.9	323.9	168.3
t (mm)	14.3	12.7	14.3
Thickness-diameter ratio (%)	4.41	3.92	8.50

6.1. Relationship between the bearing capacity and corrosion depth

This section details the impact of corrosion depth on the bearing capacity of pipelines, given a specific corrosion ratio. It illustrates the relationship between the two factors and how they interact. The relationships between the bearing capacity and corrosion depth for each section are presented in Figs. 10 and 11. As the corrosion depth and ratio increase, a noticeable decline in the bearing capacity of all three pipeline types is observed.

The relationship between bearing capacity and corrosion depth is nonlinear. As the corrosion ratio escalates, the gradient of the bearing capacity-corrosion depth ratio curve experiences a marked increase, signifying a heightened influence of corrosion depth on the pipeline's bearing capacity. Additionally, as corrosion depth intensifies, the disparity between the high and low bearing

capacity values widens. Notably, at reduced levels of corrosion, the discrepancy between the high and low bearing capacities is more pronounced compared to higher corrosion rates. This observation indicates greater uncertainty in the pipeline's bearing capacity when corrosion rates are relatively low.

Fig. 11 illustrates the correlation between bearing capacity and corrosion depth across various corrosion ratios. For Type 3, the slope of the bearing capacity-corrosion depth ratio curve is the least among the three types, regardless of whether the values are low or high. Furthermore, when the corrosion ratio is substantial, the curve of Type 1 exhibits a steeper incline compared to Type 2.

Table 7
Bearing capacity of corrosion type with different y_{max}

Corroded section model			$y_{max} = D/2$, $t = t$		$y_{max} = D/2 - t_d$, $t = t_r$		uncorroded		Thickness diameter ratio
Diameter (mm)	Thickness (mm)	Corrosion depth (mm)	Bearing capacity (kN)	Relative error (%)	Bearing capacity (kN)	Relative error (%)	Bearing capacity (kN)	Relative error (%)	—
150	30	10	642	0.00	744	15.89	846	31.78	0.2
200	30	10	954	0.00	1044	9.43	1206	26.42	0.15
200	20	10	654	0.00	690	5.50	882	34.86	0.1
400	10	3	1092	0.00	1098	0.55	1266	15.93	0.025
500	10	3	1464	0.00	1470	0.41	1710	16.80	0.02

Table 9
Design parameters of the corrosion and the high value of bearing capacity for the pipelines

Type 1				Type 2				Type 3			
t_d (mm)	ρ_{CR}	DOPs (%)	Bearing capacity (kN)	t_d (mm)	ρ_{CR}	DOPs (%)	Bearing capacity (kN)	t_d (mm)	ρ_{CR}	DOPs (%)	Bearing capacity (kN)
0.00	0	0.00	1248	0.00	0	0.00	1140	0.00	0	0.00	552
2.86	0.2	2.38	1200	2.54	0.2	2.37	1098	2.86	0.2	2.46	528
5.72	0.2	4.71	1146	5.08	0.2	4.70	1050	5.72	0.2	4.84	504
8.58	0.2	7.00	1092	7.62	0.2	6.99	990	8.58	0.2	7.13	480
11.44	0.2	9.25	996	10.16	0.2	9.24	912	11.44	0.2	9.34	450
2.86	0.4	4.75	1152	2.54	0.4	4.73	1056	2.86	0.4	4.92	528
5.72	0.4	9.42	1062	5.08	0.4	9.39	972	5.72	0.4	9.68	462
8.58	0.4	14.00	960	7.62	0.4	13.98	882	8.58	0.4	14.26	420
11.44	0.4	18.50	852	10.16	0.4	18.48	768	11.44	0.4	18.68	378
2.86	0.6	7.13	1110	2.54	0.6	7.10	1020	2.86	0.6	7.39	480
5.72	0.6	14.13	978	5.08	0.6	14.10	894	5.72	0.6	14.52	420
8.58	0.6	21.01	846	7.62	0.6	21.00	762	8.58	0.6	21.39	360
11.44	0.6	27.76	672	10.16	0.6	27.73	630	11.44	0.6	28.01	312
2.86	0.8	9.51	1068	2.54	0.8	9.47	978	2.86	0.8	9.85	462
5.72	0.8	18.84	888	5.08	0.8	18.78	810	5.72	0.8	19.36	378
8.58	0.8	28.01	696	7.62	0.8	27.95	642	8.58	0.8	28.52	312
11.44	0.8	37.01	510	10.16	0.8	36.97	474	11.44	0.8	37.35	246

Table 10
Design parameters of the corrosion and the low value of bearing capacity for the pipelines

Type 1				Type 2				Type 3			
t_d (mm)	ρ_{CR}	DOPs (%)	Bearing capacity (kN)	t_d (mm)	ρ_{CR}	DOPs (%)	Bearing capacity (kN)	t_d (mm)	ρ_{CR}	DOPs (%)	Bearing capacity (kN)
0.00	0	0.00	1248	0.00	0	0.00	1140	0.00	0	0.00	552
2.86	0.2	2.38	1206	2.54	0.2	2.37	1104	2.86	0.2	2.46	540
5.72	0.2	4.71	1164	5.08	0.2	4.70	1068	5.72	0.2	4.84	522
8.58	0.2	7.00	1116	7.62	0.2	6.99	1014	8.58	0.2	7.13	510
11.44	0.2	9.25	1032	10.16	0.2	9.24	936	11.44	0.2	9.34	486
2.86	0.4	4.75	1206	2.54	0.4	4.73	1062	2.86	0.4	4.92	516
5.72	0.4	9.42	1074	5.08	0.4	9.39	984	5.72	0.4	9.68	474
8.58	0.4	14.00	984	7.62	0.4	14.00	888	8.58	0.4	14.30	444
11.44	0.4	18.50	870	10.16	0.4	18.48	792	11.44	0.4	18.68	396
2.86	0.6	7.13	1116	2.54	0.6	7.10	1020	2.86	0.6	7.39	492
5.72	0.6	14.10	984	5.08	0.6	14.10	900	5.72	0.6	14.50	432
8.58	0.6	21.00	858	7.62	0.6	21.00	786	8.58	0.6	21.40	378
11.44	0.6	27.76	702	10.16	0.6	27.73	642	11.44	0.6	28.01	324
2.86	0.8	9.51	1074	2.54	0.8	9.47	984	2.86	0.8	9.85	468
5.72	0.8	18.84	894	5.08	0.8	18.78	822	5.72	0.8	19.36	390
8.58	0.8	28.01	720	7.62	0.8	27.95	660	8.58	0.8	28.52	318
11.44	0.8	37.01	528	10.16	0.8	36.97	492	11.44	0.8	37.35	252

The result suggests that in pipelines composed of various sections, the bearing capacity of the pipelines is increasingly affected by the depth of corrosion as the thickness-diameter ratio decreases. Notably, when the pipeline's thickness-diameter ratio is comparable, thicker walled pipelines are more susceptible to the influence of corrosion depth, particularly under conditions of high corrosion ratios. It can be seen in Fig. 11 that, for pipeline Type 3, which boasts a thicker thickness-diameter ratio compared to the other two pipelines, exhibits a substantial variance in its bearing capacity between its high and low values. It is indicated that the value of y_{max} significantly influences the pipeline's bearing capacity when considering the impact of corrosion depth.

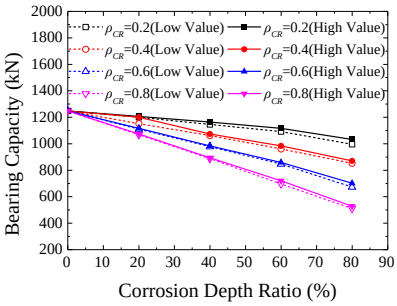

(a) Type 1

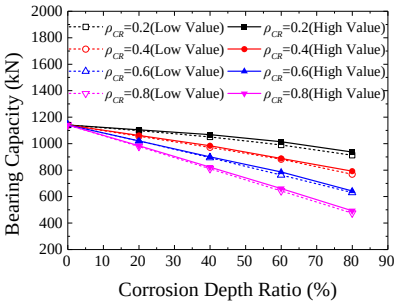

(b) Type 2

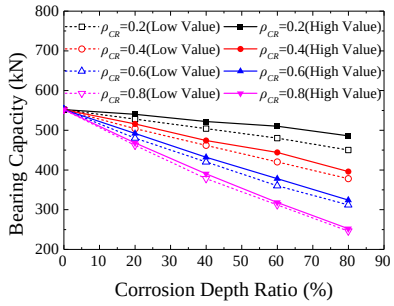

(c) Type 3

Fig. 10 The bearing capacity of three types of pipelines

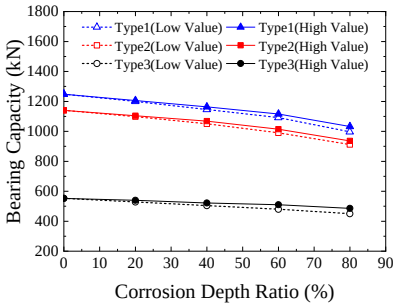

(a) Corrosion Ratio = 0.2

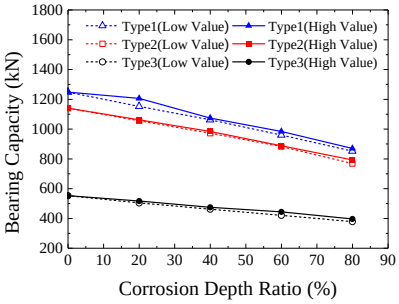

(b) Corrosion Ratio = 0.4

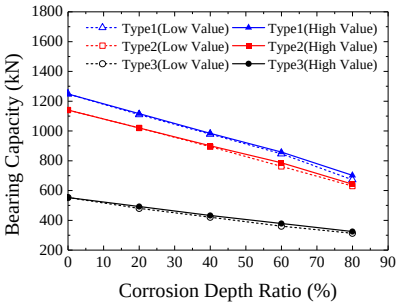

(c) Corrosion Ratio = 0.6

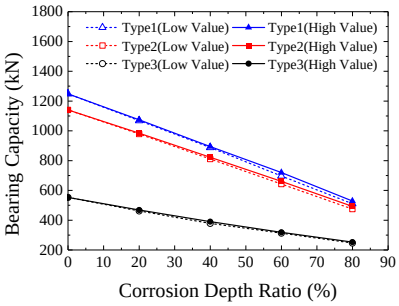

(d) Corrosion Ratio = 0.8

Fig. 11 The relationship between bearing capacity and corrosion depth

6.2. Relationship between bearing capacity and corrosion ratio

The objective of this section is to undertake a comprehensive examination of the impact exerted by the corrosion ratio on the bearing capacity of pipelines, with the corrosion depth remaining constant throughout the analysis. Fig. 12 exhibits the trend of the bearing capacity variations in three distinct pipeline types with respect to escalating corrosion ratios. As shown in Fig. 12, all three types of pipelines exhibit a decline in their bearing capacity as the corrosion ratios rise. Additionally, as the corrosion depth ratio escalates, the nonlinearity of the bearing capacity-corrosion ratio curve becomes increasingly apparent, and the slop of the curve experiences a marked increase. These observations underscore the influence of corrosion ratio on pipeline bearing capacity, particularly at deeper corrosion depths. As the corrosion ratio increases, the gap between the high and low values of pipeline bearing capacity tends to narrow. Moreover, pipelines with higher corrosion depth rates exhibit a more substantial dispersion in their bearing capacity values compared to those with lower corrosion depth rates. It can be inferred that pipelines with a lower corrosion depth ratio tend to possess a bearing capacity that is less predictable.

The relationship between the bearing capacity and the corrosion ratio for different pipeline's corrosion ratio can be seen in Fig. 13. The slope of the bearing capacity-corrosion ratio curve for Type 3 pipelines is the least steep. In contrast, Types 1 and 2 exhibit a more rapid decline in bearing capacity with increasing corrosion ratio. Furthermore, a noticeable impact of the corrosion depth ratio on the trend is observed. As the corrosion depth ratio increases, the rate of change in the curve slope among the three types of pipelines follows the order: Type 1 > Type 2 > Type 3.

The result reveals that for pipelines with a reduced thickness-diameter ratio, the influence of the corrosion ratio on the bearing capacity becomes more pronounced. Specifically, under conditions of elevated corrosion depth ratios, the thicker-walled pipelines exhibit a greater sensitivity to the corrosion ratio, particularly when the thickness-diameter ratios of the pipelines are comparable. Furthermore, it is observed that across all three types of pipelines, the disparity between the high and low values of bearing capacity remains minimal. This

suggests that the influence of y_{max} on the relationship between bearing capacity and corrosion ratio is negligible.

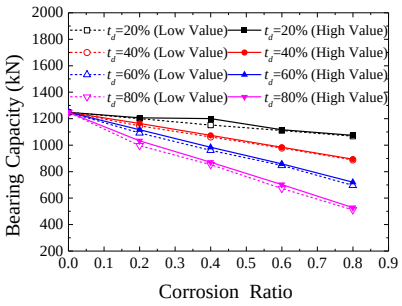

(a) Type 1

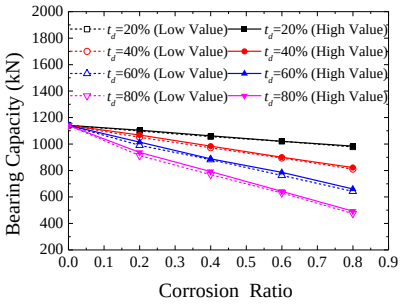

(b) Type 2

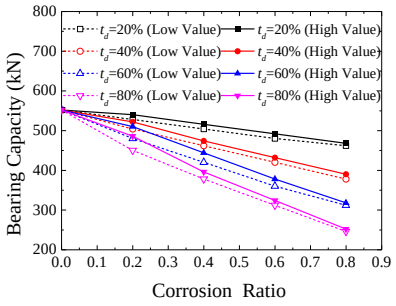

(c) Type 3

Fig. 12 The bearing capacity of three types of pipelines

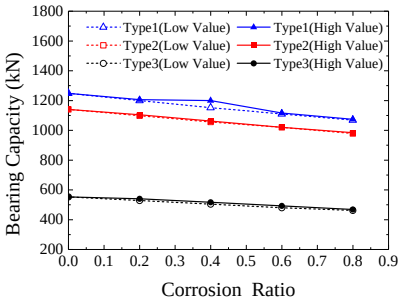

(a) Corrosion Depth Ratio = 20%

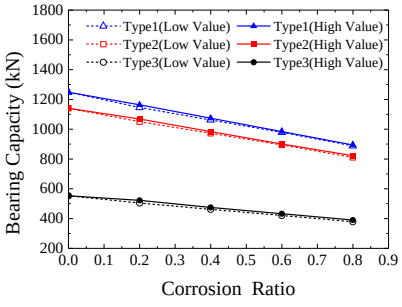

(b) Corrosion Depth Ratio = 40%

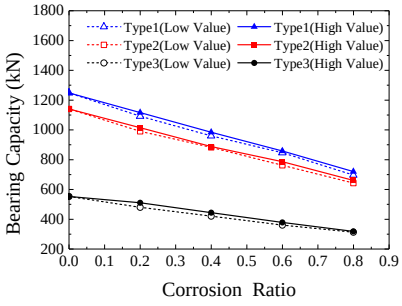

(c) Corrosion Depth Ratio = 60%

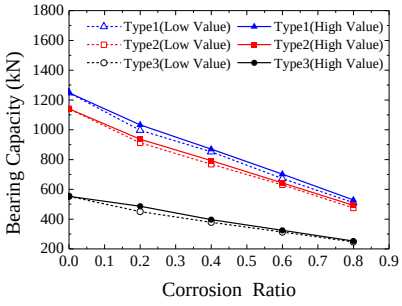

(d) Corrosion Depth Ratio = 80%

Fig. 13 The relationship between bearing capacity and the corrosion ratio

6.3. Relationship between bearing capacity and corrosion DOPs

This section aims at investigating the relationship between the pipeline's bearing capacity and the area loss ratio. Fig. 14 reveals that the bearing capacity of all three pipeline types diminishes as the DOPs increase. Moreover, the bearing capacity-DOPs curve exhibits great nonlinearity. Notably, the bearing capacity-DOPs curve of Type 3 pipeline exhibits the least variation in slope compared to Type 1 and Type 2, which display comparable patterns.

Meanwhile, it is evident that despite the proximity of area loss ratios, slight variations in bearing capacity for identical sections may occur. This variance is more pronounced in Types 1 and 2, whereas for Type 3, the fluctuations in the curve are minimal. To delve deeper into the uncertainty of pipeline bearing capacity under a specific area loss ratio, multiple scenarios with comparable DOPs values have been considered, as detailed in Tables 9 and 10. The ratio comparing the bearing capacity of a corroded pipeline to that of an intact pipeline serves as the benchmark, referred to as the reduction factor. Both the upper and lower bounds of the reduction factor, along with the maximum relative errors among various sets of reduction factors, have been computed and are presented in Table 11.

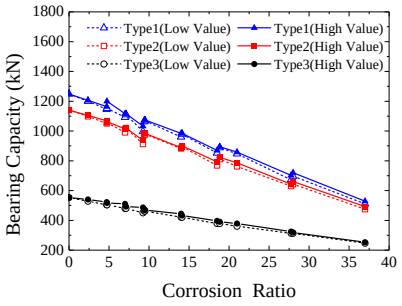

Fig. 14 Relationship between bearing capacity and DOPs

Table 11 reveals a significant variation in pipeline bearing capacity, even for identical cross-sections and area loss ratios. This variation is attributed to the combined effects of different corrosion ratio and depth. Notably, a combination of reduced corrosion depth with elevated corrosion ratio results in a more considerable reduction factor. Conversely, a scenario with deeper corrosion coupled with a lower corrosion ratio leads to a less pronounced reduction factor. These findings underscore the inadequacy of solely relying on area loss ratio to assess pipeline bearing capacity. Furthermore, they underscore the impact of corrosion on the unpredictability of pipeline bearing capacity, offering a distinct perspective on this aspect.

Upon analyzing the reduction factors across Type 1, 2, and 3 pipelines, it was evident that Types 1 and 2 exhibited significantly higher maximum relative

errors in their reduction factors compared to Type 3. Notably, pipelines of Types 1 and 2 with a smaller thickness-diameter ratio tended to possess increased uncertainty in terms of their bearing capacity when exposed to corrosion. Conversely, pipelines of Type 3 maintained consistent reduction factors in both high and low values.

Table 11 reveals that, with identical section and area loss ratios, the bearing capacity of pipelines is profoundly influenced by the intricate relationship between corrosion ratio and depth. Notably, a combination of shallow corrosion depth and high corrosion ratio results in a more pronounced reduction factor. Conversely, deeper corrosion coupled with a lower corrosion ratio leads to a less significant reduction factor. These observations underscore the inadequacy of solely relying on area loss ratio to assess pipeline bearing capacity. Furthermore, they underscore the impact of corrosion on the unpredictability of pipeline bearing capacity from a distinct perspective. When comparing the reduction factors among Type 1, 2, and 3 pipelines, it is evident that Type 1 and 2 pipelines exhibit significantly higher maximum relative errors in their reduction factors compared to Type 3. Specifically, pipelines of Types 1 and 2 with a smaller thickness-diameter ratio appear to exhibit greater uncertainty in their bearing capacity when subjected to corrosion. Conversely, Type 3 pipelines maintain consistent reduction factors across both high and low values, indicating a more reliable performance under corrosion conditions.

Table 11
The bearing capacity of 3 types of pipelines with similar DOPS

Section type	DOPs (%)	ρ_{CR}	t_d (mm)	Reduction factor (L)	Maximum relative error (%)	Reduction factor (H)	Maximum relative error (%)
	9.25	0.2	11.44	0.798		0.827	
Type 1	9.42	0.4	5.72	0.851	6.44	0.861	4.11
	9.51	0.8	2.86	0.856		0.861	
	9.24	0.2	10.16	0.800		0.821	
Type 2	9.39	0.4	5.08	0.853	6.63	0.863	3.64
	9.47	0.8	2.54	0.855		0.863	
	9.34	0.2	11.44	0.815		0.880	
Type 3	9.68	0.4	5.72	0.837	2.70	0.859	2.38
	9.85	0.8	2.86	0.837		0.848	

Table 12 presents a compilation of three distinct sets of reduction factors, each corresponding to different section types but maintaining identical DOPs, corrosion ratios, and corrosion depth ratios. The results reveal that, despite the uniformity in corrosion parameters and DOPs, there exists a noteworthy disparity in the reduction factors among the various section types. This observation underscores the limitations of solely relying on DOPs as a metric for assessing the bearing capacity of pipelines impacted by corrosion. Notably, the maximum relative error among these reduction factors can reach up to 8.3%, and there is no consistent pattern in the relationship between the reduction factors of the three section types. This implies that the section type alone is not a determinant of the magnitude of the reduction factor.

Table 12
The bearing capacity of different type of pipeline with similar DOP

DOPs (%)	ρ_{CR}	Corrosion depth ratio (%)	Section type	Reduction factor (L)	Maximum relative error (%)	Reduction factor (H)	Maximum relative error (%)
			Type 1	0.769		0.788	
14	0.4	60	Type 2	0.774	1.71	0.779	3.21
			Type 3	0.761		0.804	
			Type 1	0.678		0.688	
21	0.6	60	Type 2	0.668	3.99	0.689	0.58
			Type 3	0.652		0.685	
			Type 1	0.409		0.423	
37	0.8	80	Type 2	0.416	8.30	0.432	5.79
			Type 3	0.446		0.457	

7. Buckling deformation and stress

The section presents the global deformation, mid-span displacement and maximum stress of the section. The parameters of the pipeline are kept the same with Section 6, corrosion ratios 0.4 and 0.8, and corrosion depth ratios 40% and 80% are taken into account.

7.1. Global deformation

Fig. 15 depicts the global deformation of pipelines affected by corrosion. Given the minimal variance in vertical deformation between high and low values, only the peak vertical deformation is presented. Furthermore, the global vertical deformation of the identical type of pipeline without corrosion in the process of loading to the maximum bearing capacity is also shown in the figure as a reference. As evident from Fig. 15, as the corrosion ratio and depth increase, the pipeline's vertical deformation decreases. Concurrently, with the progression of corrosion, both the vertical deformation and the length of vertical buckling exhibit a decrease. Notably, Type 3 exhibits the largest vertical displacement, followed by Type 1, with Type 2 exhibiting the smallest displacement. It is indicated that, under specific corrosion conditions, a pipeline with a higher thickness-diameter ratio experiences more severe vertical deformation. Additionally, while the DOPs of pipelines under conditions of ρ_{CR} = 0.4, t_d = 80% and ρ_{CR} = 0.8, t_d = 40% exhibit similar trends, there are significant differences in vertical deformation for Type 1 and Type 2 pipelines between these conditions, whereas for Type 3, the difference can be neglected.

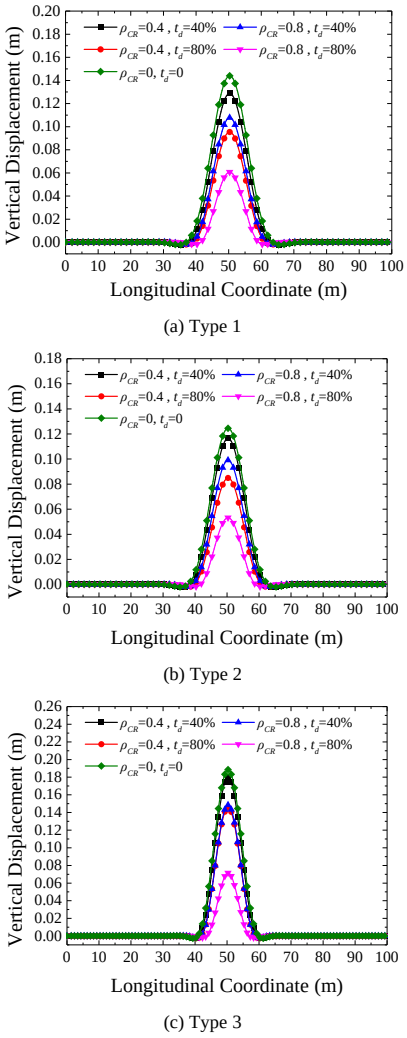

(a) Type 1

(b) Type 2

(c) Type 3

Fig. 15 The vertical deformation of the pipelines with different corrosion parameters

7.2. Vertical displacement at the midpoint

The vertical deformation at the midpoint of the pipeline exhibits a minor difference between high and low values, which is rational given the limited influence of y_{max} on the vertical deformation at the midpoint. Thus, only the high value of the vertical deformation is presented. Fig. 16 illustrates the increase in vertical displacement at the pipeline midpoint with increasing imposed load. With constant corrosion parameters, the curves exhibit a distinct nonlinearity, indicating that as external loads gradually increase and pipeline deformation accelerates, the rate of vertical displacement growth at the midpoint progressively rises. Additionally, the vertical displacement at the midpoint of

the pipeline diminishes as the corrosion ratio and corrosion depth increase, consistent with the global vertical deformation of the pipeline. Moreover, the slopes of the curves steepen correspondingly with the growth of the corrosion ratio or corrosion depth. It means that, with the aggravation of pipeline corrosion, the growth rate of vertical displacement at the midpoint increases significantly with the imposed load. Moreover, since the DOPs of the pipeline at ρ_{CR} = 0.4, t_d = 80% and ρ_{CR} = 0.8, t_d = 40% are nearly identical, resulting in similar slopes for these two curves.This supports the inference that as DOPs increase, the rate of vertical displacement growth at the midpoint responds significantly to external loads. The observed correlation between the vertical displacement at the midpoint and vertical deformation of the three pipeline types confirms that thicker sections of the pipeline exhibit more pronounced vertical deformation compared to thinner sections under comparable constant parameter conditions.

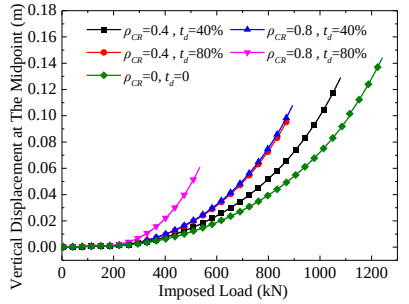

(a) Type 1

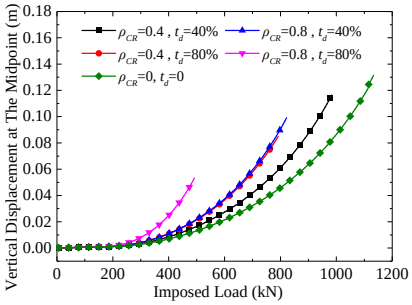

(b) Type 2

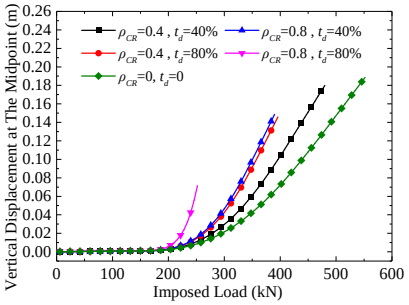

(c) Type 3

Fig. 16 The vertical displacement at the midpoint with different corrosion parameters

7.3. Stress at the midpoint

A graphical representation of the normal stress variations within the cross-section at the pipeline's midpoint, corresponding to different loading stages, is depicted in Fig. 17. Additionally, a reference value of 0.54S_y is included as the upper limit for longitudinal stress. Under imposed loads, both the stress and vertical displacement at the pipeline's midpoint exhibit comparable patterns of variation.

The stress at the midpoint of the pipeline diminishes as the corrosion ratio and depth increase. Furthermore, the slopes of the curves also increase with the corrosion ratio (corrosion depth). Moreover, when subjected to imposed loads, the stress growth rate at the midpoint experiences a notable acceleration with the elevation of DOPs. This suggests that the rate at which stress accumulates at the midpoint remarkably amplifies with the progression of pipeline corrosion. Nevertheless,the vertical displacement change at the same point exceeds the stress variation during the application of external loads, suggesting that the rate of stress accumulation at the midpoint rises steadily with the persistent imposition of external loads. Although the stresses at the midpoint are comparable among the three pipeline types, Type 3 exhibits the highest rate of stress accumulation at the midpoint, followed by Type 2, with Type 1 showing a relatively lower increase rate. Therefore, it seems that the thickness-diameter ratio of the pipeline section does not largely affect the connection between corrosion and stress at the midpoint.

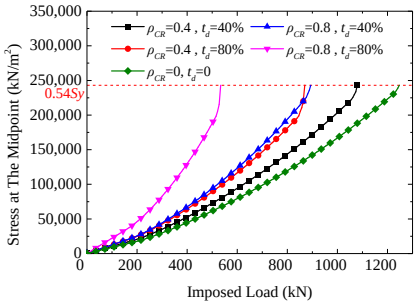

(a) Type 1

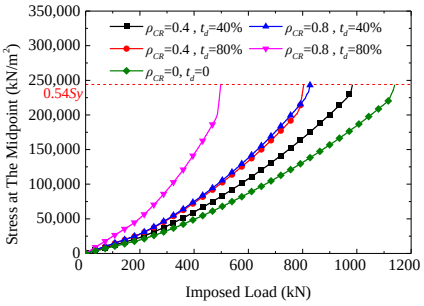

(b) Type 2

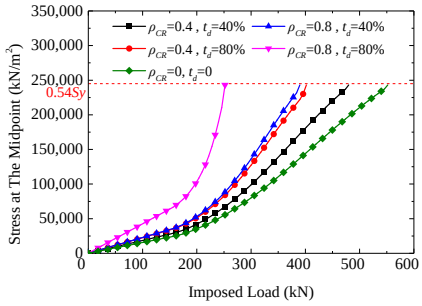

(c) Type 3

Fig. 17 The stress at the midpoint of pipelines with different corrosion parameters

8. Conclusions

By implementing Monte Carlo method, a corrosion-inclusive model of a submarine pipeline was developed to perform a numerical analysis regarding pipeline buckling considerations. The findings of this study serve as the foundation for a quantitative assessment of the pipelines' bearing capacity. Based on the previously established pipeline element, the newly introduced element demonstrates significant efficiency advantages when dealing with numerous cases that require analysis. Without the employment of highly efficient numerical models, it would be unfeasible to carry out the multi-factorial parametric studies. In order to investigate how the corrosion features affect the bearing capacity of the pipelines, a series of pitting corrosion are designed and randomly distributed across the cross sections of the pipelines. A comprehensive analysis has been conducted to assess the impact of diverse corrosion parameters, including corrosion depth, corrosion ratio, and area loss ratio, on the mechanical characteristics of pipelines. The examination encompassed key properties such as bearing capacity, buckling deformation, and stress. The findings can be summarized as follows:

- As the corrosion depth (corrosion ratio) increases, its impact on the pipelines bearing capacity becomes more increasingly significant. Even slight corrosion enhance the unpredictability of the pipeline’ s bearing capacity. With the aggravation of the corrosion, the buckling displacement and stress at the midpoint of the pipeline accelerate under applied loads, indicating accelerated deformation. Besides, pitting corrosion has a more substantial influence on the magnitude of upheaval buckling deformation than the buckling length. Evaluating the bearing

capacity of a corroded pipeline solely based on single corrosion parameter is inadequate. Minor variations in corrosion ratio and depth can lead to slight differences in the bearing capacity and buckling displacement of a specific section, especially at similar area loss ratio of the section (DOPs).The combination of substantial corrosion depth with a relatively low corrosion ratio often results in a more minor reduction in the reduction factor. Furthermore, different types of sections, even with identical corrosion parameters, can exhibit varying reduction factors and vertical buckling displacements.

- The bearing capacity of the pipeline decreases as the slenderness increases and then gradually stabilizes. When assessing the buckling bearing capacity of a corroded pipeline, it is crucial to note that the section coefficient W_Z for corroded pipelines is not clearly defined in relevant specifications. To capture the uncertainty of its bearing capacity, it is necessary to consider both values of y_{max}: $D/2$ and $D/2$- t_d. Although the effect of y_{max} on the bearing capacity and buckling deformation is limited by the impact of corrosion ratio, its influence on corrosion depth remains significant. Furthermore, the buckling bearing capacity of a pipeline can vary significantly depending on corrosion distribution. Among various corrosion models with identical area loss ratios, pipelines exhibiting regular and random corrosion patterns exhibit similar bearing capacities while the corrosion concentration in the top or bottom half of the pipeline cross-section should be avoided, as this leads to the lowest buckling bearing capacity.
- This method is applicable for corrosion analysis of both thin and thick-walled pipelines. For pipelines with varying cross-sections, a reduced thickness-to-diameter ratio leads to heightened uncertainty regarding the structural integrity of the pipeline, considering both corrosion depth and corrosion ratio. Among pipelines with similar thickness-to-diameter ratios, those with thicker walls are more vulnerable to the effects of high-level corrosion, either in terms of corrosion depth or corrosion ratio. Conversely, pipeline sections with a larger thickness-to-diameter ratio may exhibit more pronounced vertical buckling displacement under certain corrosion conditions, whereas the thickness-diameter ratio has limited impact on the relationship between corrosion and stress at the midpoint.

Acknowledgement

The corresponding author would like to express his gratitude to the Natural Science Foundation of Guangdong Province (No. 2021A1515011734), Guangdong Basic and Applied Basic Research Foundation (No. 2022B1515250002), and the third author would like to express his gratitude to the National Science Foundation, China through the project (Grant No. 52008410) and the Hong Kong SAR Government on the project Second-order direct analysis for the design of steel members with irregular cross-sections (PolyU 15203121/22E).

References

[1] Cai, J., Jiang, X. L., Lodewijks, G., 2017. Residual ultimate strength of off- shore metallic pipelines with structural damage–a literature review. Ships and Offshore Structures 12 (8), 1037–1055.

[2] Galgoul, N. S., Lupinacci Massa, A. L., Claro, C. u. A., 2004. A discussion on how internal pressure is treated in offshore pipeline design. In: Inter- national Pipeline Conference. Vol. 41766. pp. 1887–1890.

[3] Wang, R. H., Shenoi, R. A., 2019. Experimental and numerical study on ultimate strength of steel tubular members with pitting corrosion damage. Marine Structures 64, 124–137.

[4] Chen, Z. H., Yang, J. G., Wang, Z. k., 2020. Numerical study on upheaval buckling for surface laid subsea pipelines with topographic step imperfec- tion. Applied Ocean Research 101, 102232.

[5] Det Norske Veritas, 2018. Global buckling of submarine pipelines. DNV-RP- F110, Oslo, Norway.

[6] Wang, R. H., Guo, H. C., Shenoi, R. A., 2020. Compressive strength of tubular members with localized pitting damage considering variation of corrosion features. Marine Structures 73, 102805.

[7] Cosham, A., Hopkins, P., 2004. The assessment of corrosion in pipelines– guidance in the pipeline defect assessment manual (PDAM). In: Pipeline pigging and integrity management conference, Amsterdam, The Nether- lands. pp. 17–18.

[8] Netto, T. A., 2009. On the effect of narrow and long corrosion defects on the collapse pressure of pipelines. Applied ocean research 31 (2), 75–81.

[9] Wang, H., Yu, Y., Yu, J., Duan, J., Zhang, Y., Li, Z., Wang, C., 2018a.Effect of 3d random pitting defects on the collapse pressure of pipepart i: Experiment. Thin-Walled Structures 129, 512–526.

[10] Motta, R. S., Cabral, H. L., Afonso, S. M., Willmersdorf, R. B., Bouchon- neau, N., Lyra, P. R., de Andrade, E. Q., 2017. Comparative studies for failure pressure prediction of corroded pipelines. Engineering Failure Anal- ysis 81, 178–192.

[11] Mohd, M. H., Lee, B. J., Cui, Y., Paik, J. K., 2015. Residual strength of cor- roded subsea pipelines subject to combined internal pressure and bending moment. Ships and offshore Structures 10 (5), 554–564.

[12] Nazaria, M., Khedmati, M. R., Khalaj, A. F., 2014. A numerical investi- gation into ultimate strength and buckling behavior of locally corroded steel tubular members. Latin American Journal of Solids and Structures 11, 1063–1076.

[13] Ahn, J. H., Choi, W. R., Jeon, S. H., Kim, S. H., Kim, I. T., 2016. Residual compressive strength of inclined steel tubular members with local corro- sion. Applied Ocean Research 59, 498–509.

[14] Melchers, R. E., 2005a. Statistical characterization of pitting corrosion part 1: Data analysis. Corrosion 61 (07).

[15] Melchers, R. E., 2005b. Statistical characterization of pitting corrosionpart 2: Probabilistic modeling for maximum pit depth. Corrosion 61 (8), 766–777.

[16] Yamamoto, N., 2008. Probabilistic model of pitting corrosion and the simula- tion of pitted corroded condition. In: International Conference on Offshore Mechanics and Arctic Engineering. Vol. 48197. pp. 527–534.

[17] Chen, L., Liu, S. W., Zhang, J. Z., Yam, M. C. H., 2022. Efficient algorithm for elastic buckling of corroded i-section steel members with monte carlo simulation. Thin-Walled Structures 175, 109216.

[18] Silva, J. E., Garbatov, Y., Soares, C. G., 2013. Ultimate strength assess- ment of rectangular steel plates subjected to a random localised corrosion degradation. Engineering Structures 52, 295–305.

[19] Wang, R., Shenoi, R. A., Sobey, A., 2018b. Ultimate strength assessment of plated steel structures with random pitting corrosion damage. Journal of Constructional Steel Research 143, 331–342.

[20] Ben Seghier, M. e. A., Bettayeb, M., Correia, J., De Jesus, A., Cal¸cada, R., 2018. Structural reliability of corroded pipeline using the so-called separa- ble monte carlo method. The Journal of Strain Analysis for Engineering Design 53 (8), 730–737.

[21] Caleyo, F., Vel´azquez, J., Valor, A., Hallen, J. M., 2009. Probability distri- bution of pitting corrosion depth and rate in underground pipelines: A monte carlo study. Corrosion Science 51 (9), 1925–1934.

[22] Wu, X., Lu, H., Wu, S., 2015. Stress analysis of parallel oil and gas steel pipelines in inclined tunnels. SpringerPlus 4 (1), 1–25.

[23] Khakimov, A., 2018. Interaction of pipeline instabilities. In: AIP Conference Proceedings. Vol. 2053. AIP Publishing LLC, p. 030025.

[24] Liu, R., Li, C. F., 2018. Determinate dimension of numerical simulation model in submarine pipeline global buckling analysis. Ocean Engineering 152, 26–35.

[25] Ma, H. H., Li, B. E., 2023. CFD-CGDEM coupling model for scour process simulation of submarine pipelines. Ocean Engineering 271, 113789.

[26] Ning, J., Lin, T., Liu, S., Bai, R., Huang, W., 2023. Three-dimensional pipeline element formulation for global buckling analysis of submarine pipelines with sleeper. Marine Structures 90, 103428.

[27] Ning, J. H., Liu, S. W., Lin, T., Huang, W., 2022. Pipeline elemen- t for upheaval buckling analysis of submarine pipelines with geometric- imperfections under high temperature high pressure. Ocean Engineering 264, 112456.

[28] Ning, J. H., Liu, S. W., Wan, J. H., Huang, W., 2021. Line-element for- mulation for upheaval buckling analysis of buried subsea pipelines due to thermal expansion. Advanced Steel Construction 17 (2), 210–220.

[29] Mateus, A. F., Witz, J. A., 1998. On the post-buckling of corroded steel plates used in marine structures. RINA Trans 140, 165–183.

[30] Cumming, G., Rathbone, A., 2010. Euler buckling of idealised horizontal pipeline imperfections. In: International Conference on Offshore Mechanics and Arctic Engineering. Vol. 49132. pp. 293–300.

[31] Markov, E. V., Pulnikov, S. A., Sysoev, Y. S., Kazakova, N. V., 2018. The convergence rate of the euler model for the deformed state when calculating the longitudinal bending. International Journal of Civil Engineering and Technology 9 (10), 1974–1979.

[32] American National Standards Institute, 2022. Pipeline transportation sys- tems for liquid hydrocarbons and other liquids. American Society of Me- chanical Engineers.